GEOPHYSICAL INSTITUTE

of the

UNIVERSITY OF ALASKA

Final Report

Grant NGR 02-001-099, Supplement No. 2

Prepared for

National Aeronautics and Space Administration

and Presented as two papers

to IAGA, Sept. 1973

February 1974

G. G. Sivjee
Principal Investigator

Keith B. Mather
Director
Geophysical Institute

Page Intentionally Left Blank

N74-22037

COORDINATED ANALYSIS OF AIRBORNE SPECTROPHOTOMETRIC MEASUREMENTS FROM THE MID-DAY AURORAS

G. G. Sivjee
Geophysical Institute
University of Alaska
Fairbanks, Alaska 99701

Early in 1968 and again towards the end of 1969, the National Aeronautics and Space Administration of USA sponsored a total of forty-two air flights in mid- and high-latitude areas specifically for studying atmospheric emissions from the nightglow and the aurora, as well as events related to magnetic substorms.[1] Several universities and national as well as industrial research laboratories participated in these missions, employing a sophisticated array of photometers, spectrometers, all-sky cameras, TV cameras, radiometers, riometers and magnetometers to monitor various high altitude atmospheric phenomena from an airborne platform. While some participants in the expedition have reported their findings in the literature, little effort has been expended in correlated analysis of the massive wealth of data gathered from the airborne measurements. The aeronomy group at the Geophysical Institute of the University of Alaska is currently attempting such correlated analysis under a NASA rsearch grant, and this morning I would like to present to you some preliminary results of our efforts in this area.

The data we have analyzed so far come from a half meter Ebert spectrophotometer, several fixed and tilting interference-filter photometers and all-sky cameras. In particular we have looked at measurements made with these detectors in the mid-day auroras and compared them with similar

measurements from the night-time auroras. Figure 1 shows a single scan output of the spectrometer taken around Fort Churchill in a westward travelling surge. This spectrum of the auroral emissions in the 3000 to 4000 A is a representative sample of the several hundred spectra in this wavelength region obtained in night-time auroras. The most prominent auroral emission features in this UV spectrum are the N_2^+ING, the $N_2$2PG, and N_2VK bands as well as some atomic oxygen and nitrogen lines. Please note the relative intensities of the (0-0) and (1-1) bands of N_2^+ING system in this spectrum. It is apparent that the (0-0) band is many times brighter than the (1-1) band, in conformity with the ratio of population-weighted Frank-Condon factors for the transitions involved. To demonstrate this more clearly nine scans were summed to obtain the spectral profiles of the N_2^+ING (0-0) and (1-1) bands shown in Figure 2. The solid curve is the observed auroral spectrum while the dashed curve represents a synthetic spectrum constructed assuming 5A resolution for the spectrometer and vibrational and rotational temperatures of 0 and 250°Ks respectively. While no elaborate care has been taken in comparing the two spectra, a simple visual matching shows that the observed intensity distribution of these two bands do indeed correspond to the case where all N_2 molecules are in the lowest vibrational level and the rotational levels of the electronic ground state are populated according to a Boltzman distribution characterized by a rotational temperature of about 250°K. The ratio of the population weighted Frank-Condon factors for the transitions which produce the (0-0) and (1-1) bands of N_2^+ING is approximately 24.

I would now like to discuss some of the data obtained from the mid-day auroras. During two flights from Norway to Greenland and back, the aircraft,

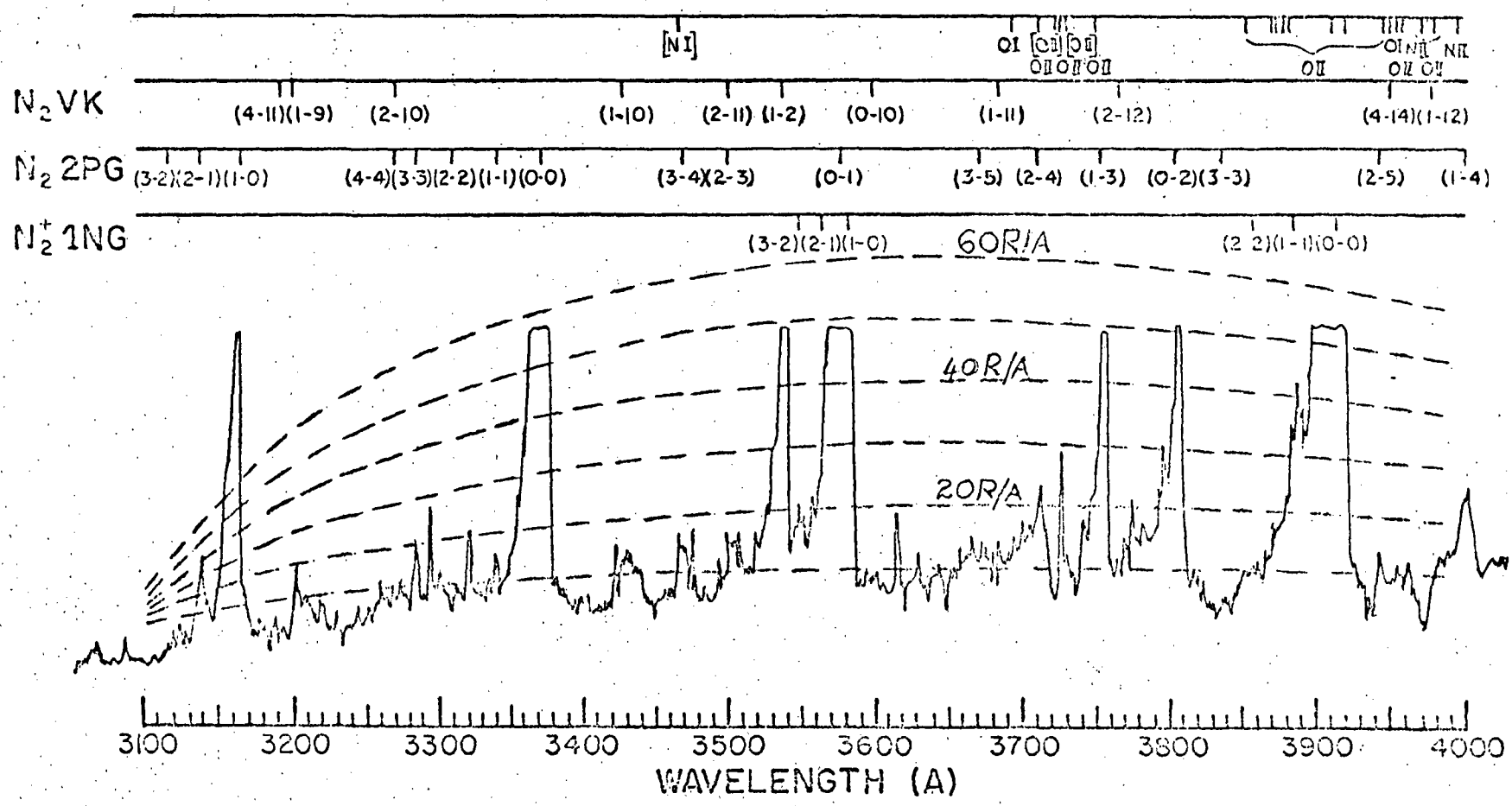
[N I]
O I
O II O II O II
O II
O I N II
N II
O II O II
N_2 VK
(4-11)(1-9)
(2-10)
(1-10)
(2-11) (1-2)
(0-10)
(1-11)
(2-12)
(4-14)(1-12)
N_2 2PG
(3-2)(2-1)(1-0)
(4-4)(3-3)(2-2)(1-1)(0-0)
(3-4)(2-3)
(0-1)
(3-5)
(2-4)
(1-3)
(0-2)(3-3)
(2-5)
(1-4)
N_2^+ 1NG
(3-2)(2-1)(1-0)
60R/A
(2 2)(1-1)(0-0)
40R/A
20R/A
3100
3200
3300
3400
3500
3600
3700
3800
3900
4000
WAVELENGTH (A)

Figure 1

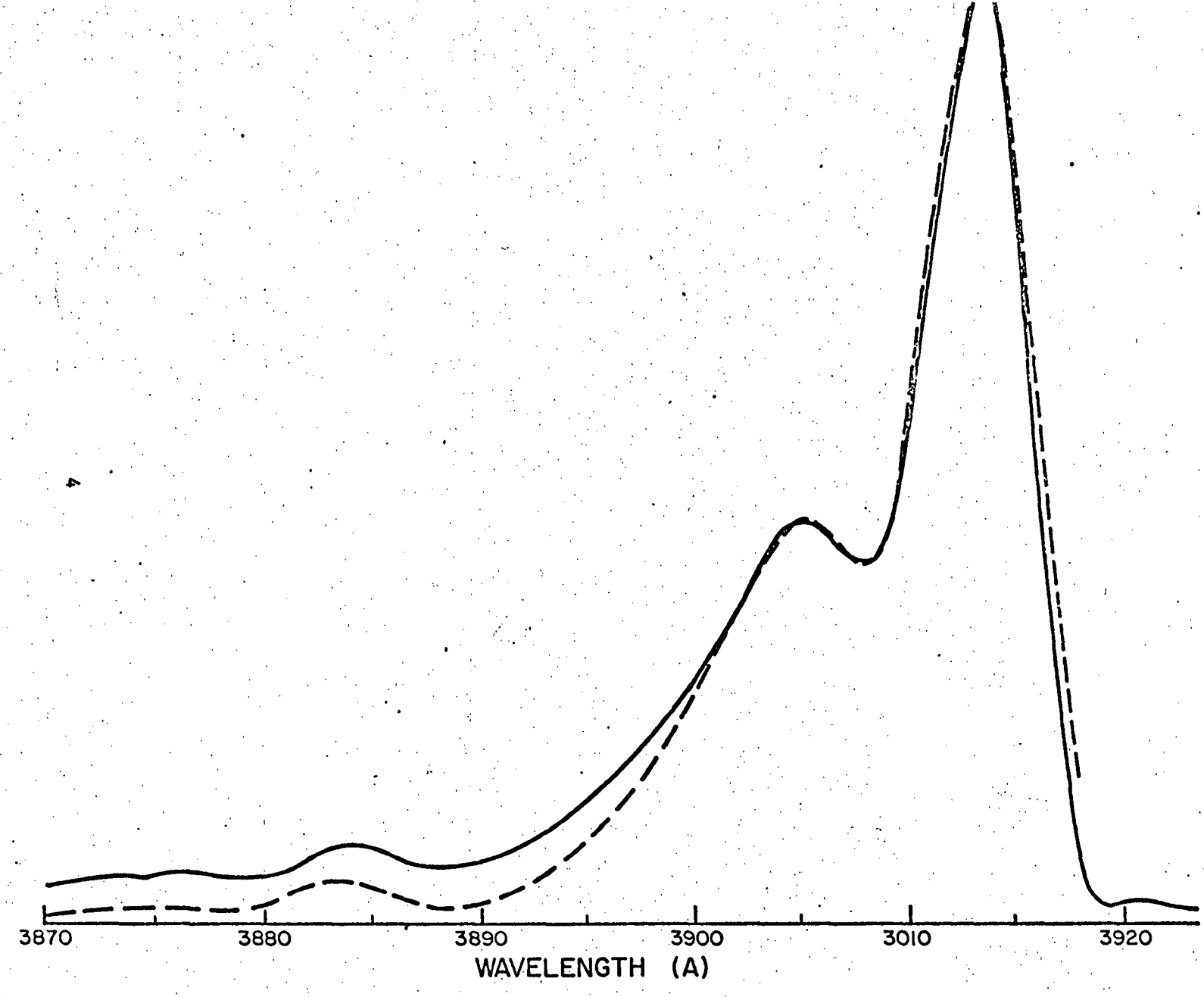

Figure 2

a Convair 990, flew under several weak and patchy red auroras around the mid-day section of the oval. An all-sky camera picture of one such aurora observed at 0845 around IL 80° (Geog. lat. = 79°, Long. = 25°W) is shown in Figure 3. The airplane was flying along a direction slightly north of west, and the zenith detectors scanned across the auroral patches, shown here, as the aircraft passed under these auroras. Measurements made with a fixed multichannel photometer, having the same field of view as the spectrometer, are presented in Figure 4 which shows the variations in the intensities of the green and red lines of atomic oxygen as well as the intensities of the N_2^+ING(0-1) and $N_2$2PG (0-0) bands. These measurements were made over the area spanning the invariant latitude from approximately 75° to 82°. Judging by the relative intensities of the emissions monitored and the morphology of magnetospheric charged particles reported in the literature, we infer that the flight path crossed over from the trapping region through the trapping boundary and into the cusp region. The ratios of 6300 to 5577 and 4278 changed from about 0.4 and 2.7 equatorward of the trapping boundary to 1.3 and 9.0 in the trapping boundary and thence to 4.4 and 25.9 in the cusp region. The dashed lines in Figure 4 enclose the region in which the N_2^+ING band measurements from the half-meter spectrometer were averaged. Before presenting these measurements, I would like to show the data from several tilting photometers taken in this same aurora. Figure 5 presents the variations in the intensities of the red and green line of atomic oxygen, the Balmer β line of atomic hydrogen and the (0-1) band of N_2^+ING. The geometrical shadow height, which varied from 270 km to 370 km in the period bounded by the dashed line, is also

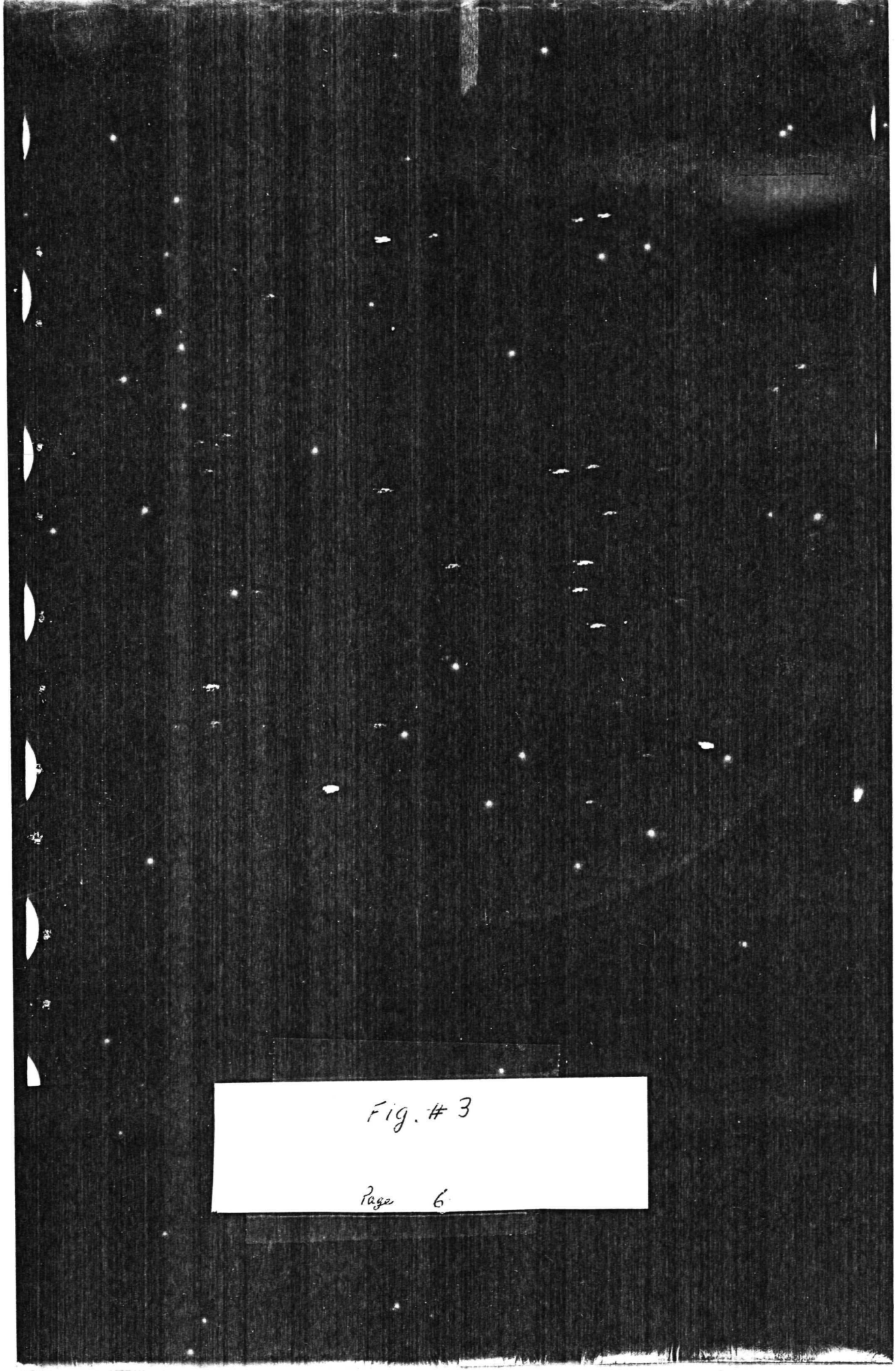

Fig. # 3

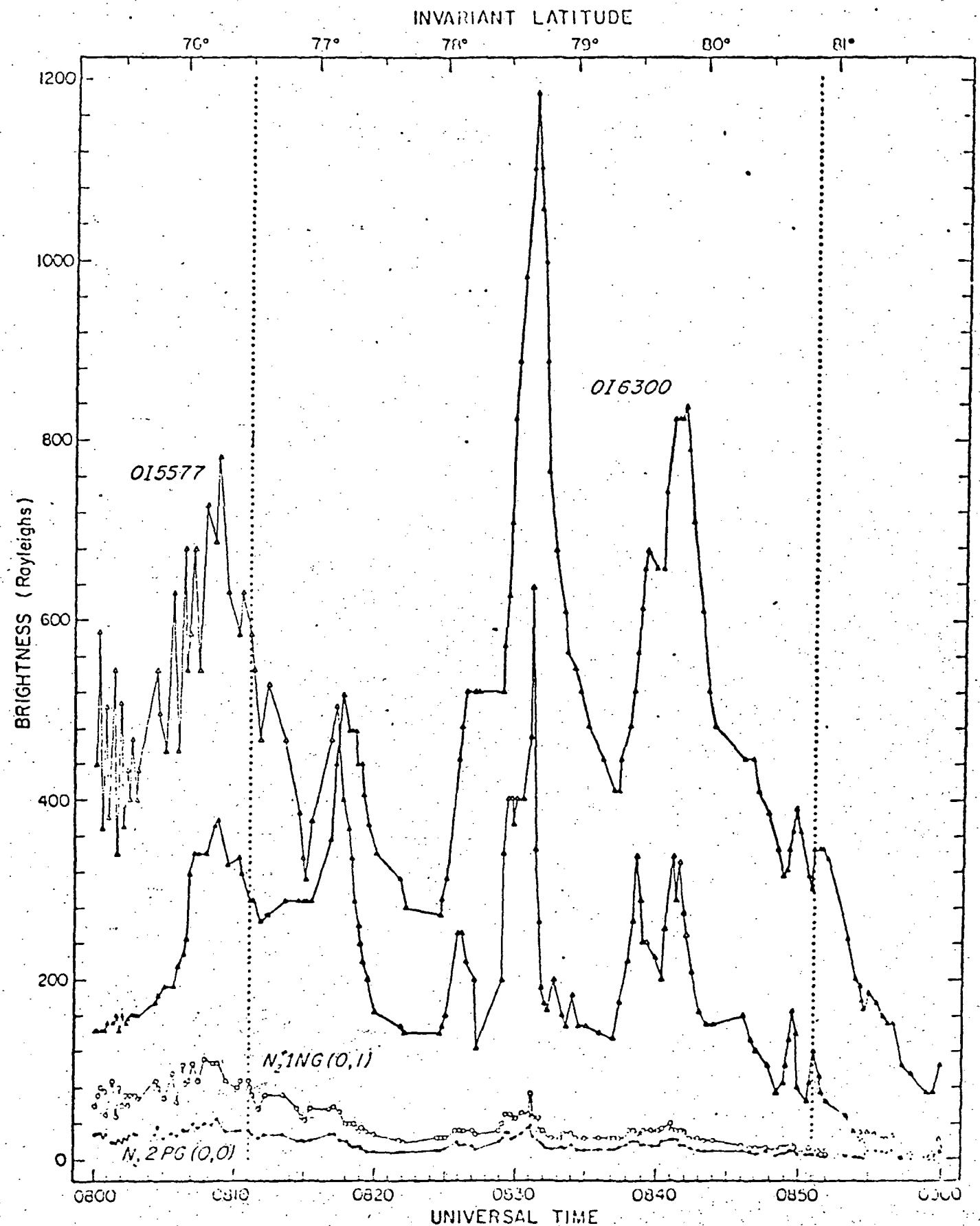
INVARIANT LATITUDE
76°
77°
78°
79°
80°
81°
1200
1000
800
600
400
200
0
BRIGHTNESS (Rayleighs)
015577
016300
N2 1NG (0,1)
N2 2PG (0,0)
0800
0810
0820
0830
0840
0850
0900
UNIVERSAL TIME

Figure 4

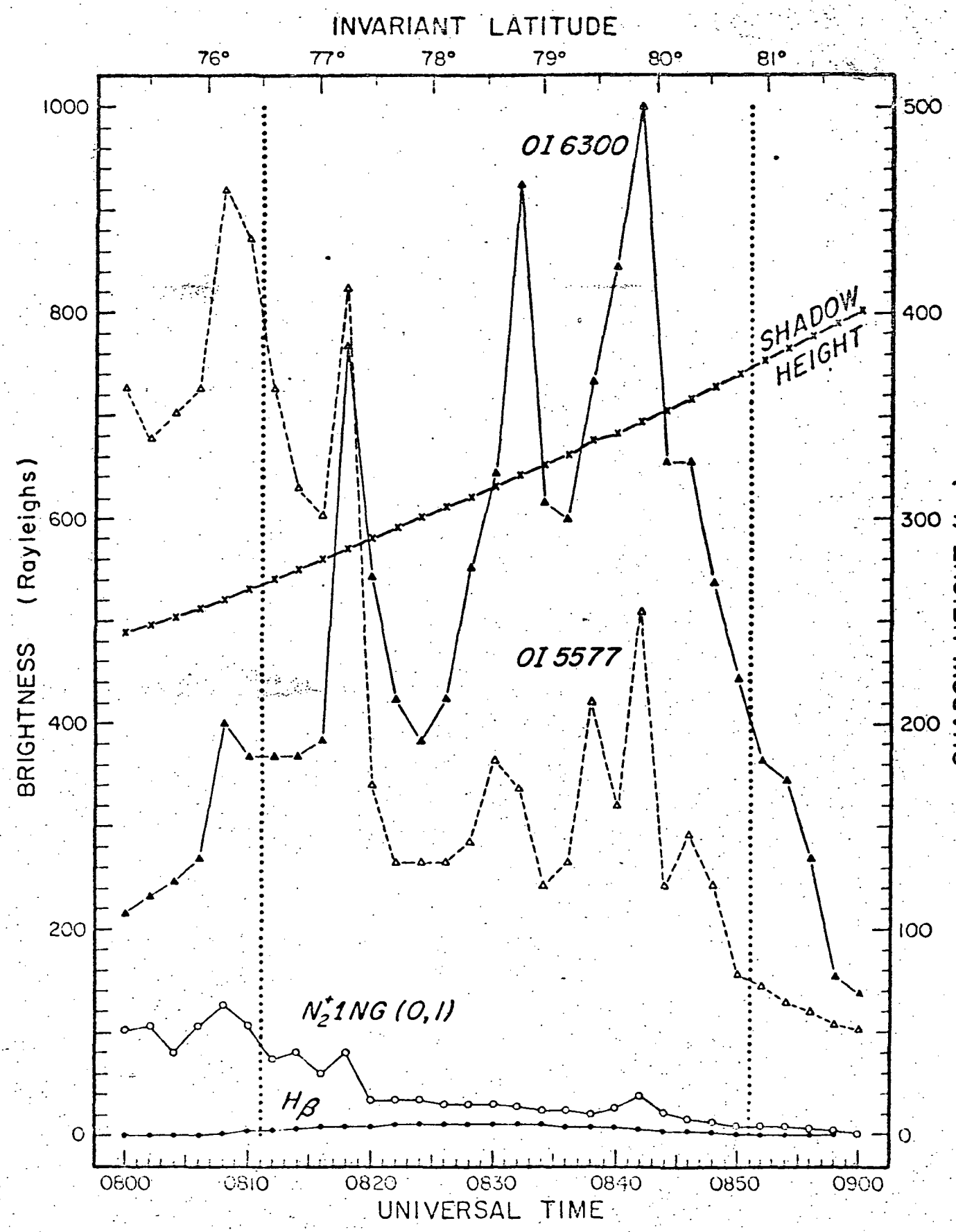
INVARIANT LATITUDE
76°
77°
78°
79°
80°
81°
1000
800
600
400
200
0
500
400
300
200
100
0
BRIGHTNESS (Rayleighs)
SHADOW HEIGHT (km)
O1 6300
SHADOW HEIGHT
O1 5577
N_2^+1NG (0,1)
Hβ
0800
0810
0820
0830
0840
0850
0900
UNIVERSAL TIME

Figure 5

shown. The solar depression angle varied from about 16° to 19° during the time in which the spectral data were averaged. Also, please note the appearance of hydrogen emission during this period; the H_β brightness in the cusp region attained a peak value of about 10R.

Two spectra of the auroral optical emissions, in the 3000 to 4000A region, from a mid-day aurora are shown in the next Figure 6. Comparing the relative intensities of the (0-0) to (1-1) bands we see that this ratio is much smaller than the value of about 24 found in the night-time auroras. This is more clearly seen by adding several spectra and displaying only these two bands. The next diagram (Figure 7) shows the result of adding all spectrometer scans obtained between IL 76.5° and 81°. Comparing the intensity of the (1-1) band to the (0-0) we clearly see a relative brightening of the (1-1) band in the mid-day aurora. The ratio of the (0-0) to (1-1) band intensities is about 8, i.e., a factor of 3 lower than the value observed in the night-time auroral spectrum shown earlier. In an attempt to determine the rotational temperature of the (0-0) band we have constructed synthetic spectra of the N_2^+ING (0-0) and (1-1) bands at various rotational temperatures for a fixed vibrational temperature of 0°K. One such synthetic spectrum at 3500°K is shown in Figure 7. Clearly the rotational temperature of the first negative bands of N_2^+ is higher than 3500°K and the vibrational temperatures of N_2 must be much higher than 0°K at atmospheric altitudes where optical emissions from mid-day auroras peak.

In attempting to understand the mechanism which causes such an anomalous intensity distribution of the N_2^+ING bands we note from Heikkila and Winningham's

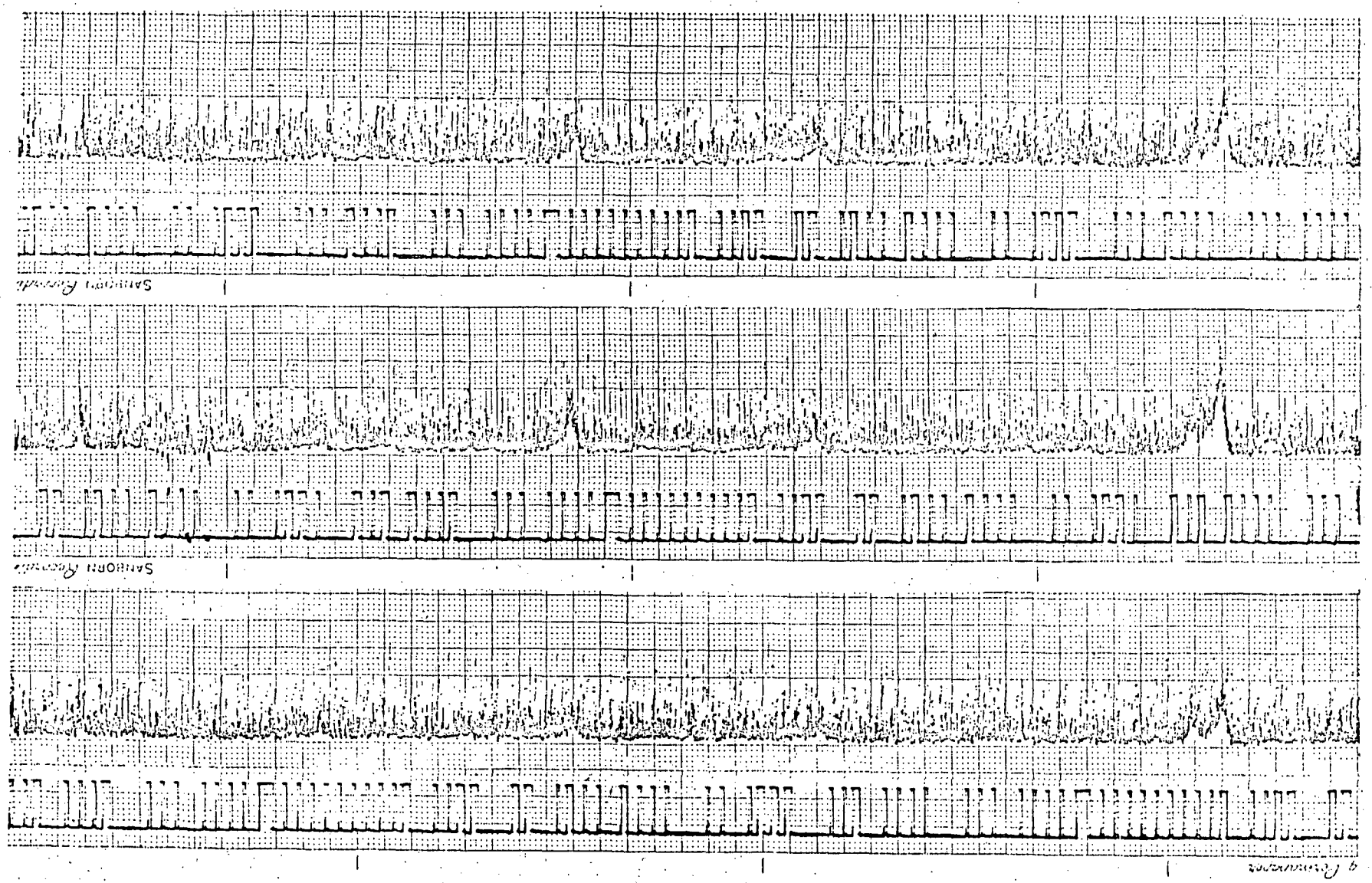

Fig. 6

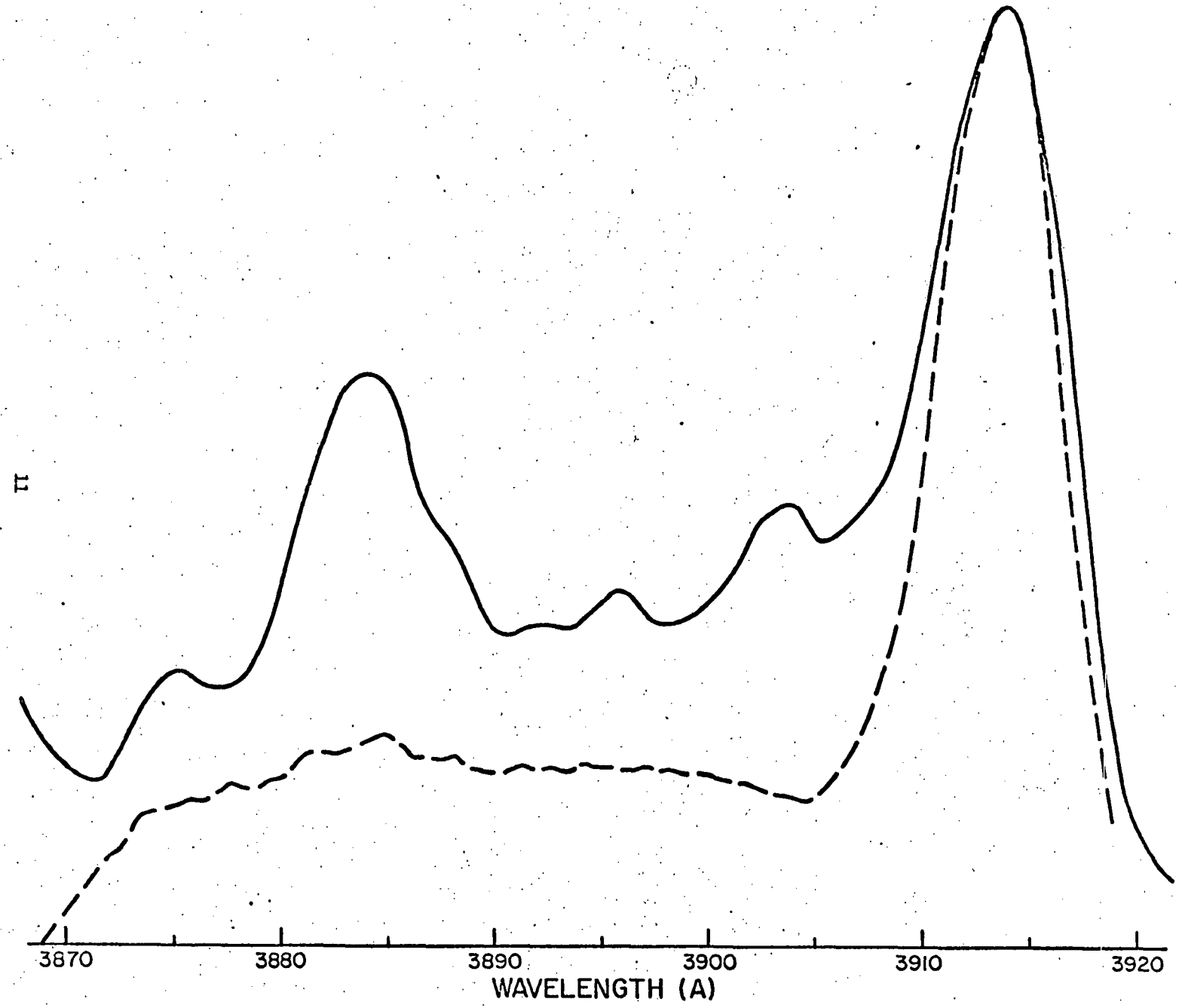

Figure 7

measurements of the particle flux in the cusp region that during magnetically quiet periods the electrons have characteristic energies of around 100 to 200 eV while the proton energy is between 300 eV and 1 keV. These particles will be stopped in the F region[3] where most of the optical emissions in mid-day auroras must therefore originate. This inference is supported by the airborne photometric observations showing high ratios of 6300 to 5577 and 4278 in mid-day auroras. The high altitude of these auroras suggests several mechanisms which could produce an intensity distribution of N_2^+ING bands markedly different from the values observed in the relatively low altitude night-time auroras.

Calculations made by Walker et al.[4], Jamshidi[5], and Bauer et al.[6], predict a vibrational temperature of N_2 ground state much higher than the translational temperature in the lower thermosphere. Recent calculations of Breig et al.[7] which take into consideration the effect of quenching of N_2 by atomic oxygen give values ranging from 800 to 2200° for the vibrational temperature of N_2 in the 200 to 300 km altitude region of the atmosphere. To find the N_2 vibrational temperature which would produce a ratio of 8 between the intensities of N_2^+ING (0-0) and (1-1) bands we have calculated the ratios of the population-weighted Frank-Condon factors for these emissions and the results are displayed in Figure 8. The observed ratio of about 8 in mid-day auroras corresponds to N_2 vibrational temperature of around 2600°K. However, as we saw in the last diagram, the observed rotational temperature is in excess of 3500°K whereas the translational temperature in the F region is about 800°K. Hence, while this effect may

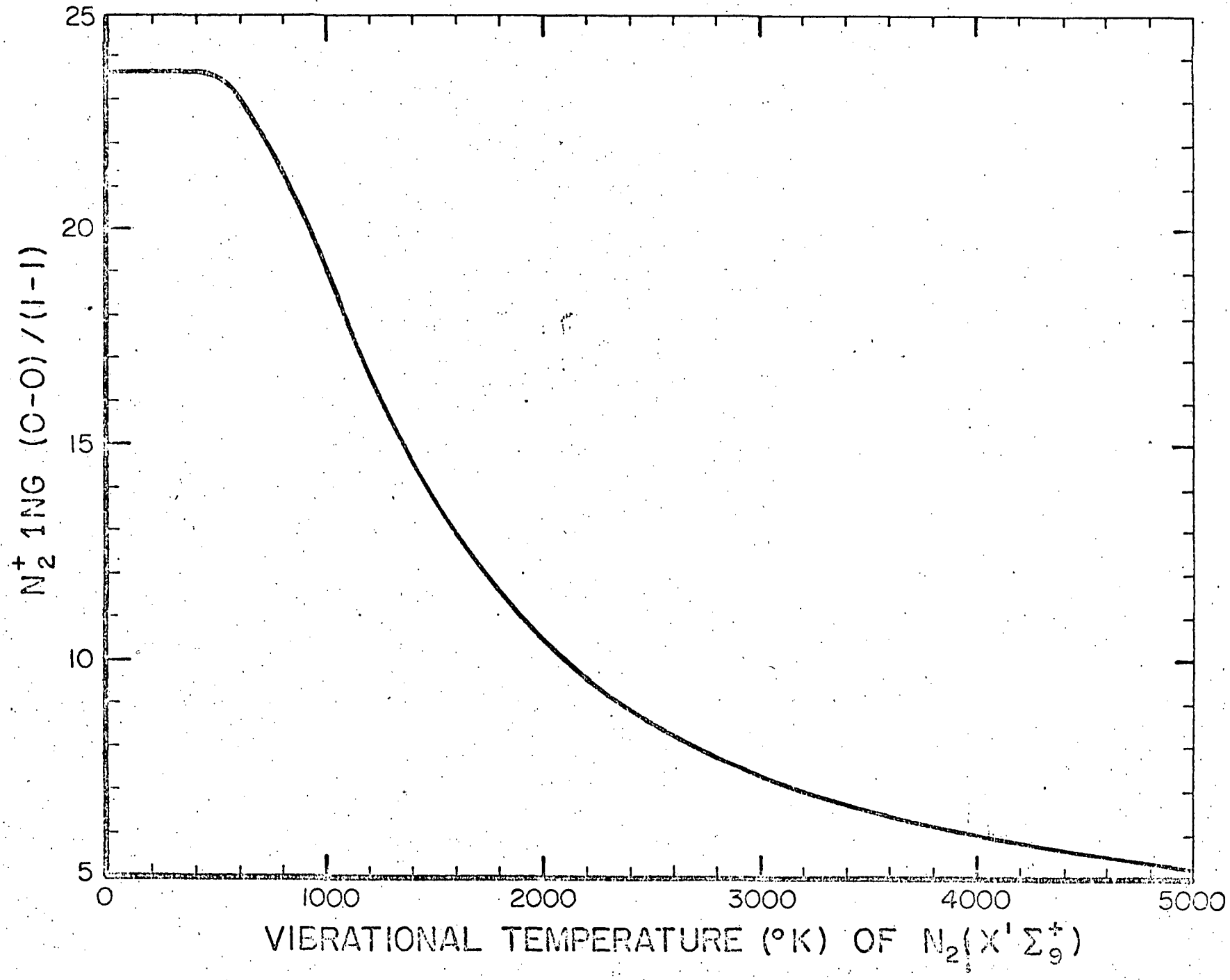
25
20
15
10
5
0
1000
2000
3000
4000
5000
N_2^+ 1NG (0-0) / (1-1)
VIBRATIONAL TEMPERATURE (°K) OF $N_2(X'\Sigma_g^+)$

Figure 8

contribute to the lowering of the (0-0) to (1-1) band-intensities ratio, it cannot increase the rotational temperature from 800° to more than 3500°K.

A second mechanism is resonant scattering of solar radiation. Vallance Jones and Hunten[8] observed a ratio of 100:26 for the intensities of the (0-1) and (1-2) bands of N_2^+ING in sunlit auroras peaked around 400 to 500 km, compared to the ratio of 100:11 for non-sunlit aurora. Relative to the (0-1) band the intensity of the (1-2) band was higher by a factor of 2 in sunlit aurora and the rotational temperature was around 2200°K. On the other hand Broadfoot and Hunten[9] in their studies of the twilight emissions of N_2^+ING (0-0) and (1-1) bands, peaking around 255 km, did not observe a very drastic change in the ratio of the (0-0) to (1-1) band intensities and the (0-0) band profile fitted a synthetic spectrum for 1600°K. Satellite particle data from the cusp region[2] as well as the observed ratio of 6300 to 4278 in mid-day auroras suggest that the auroral particles in this region penetrate down to 200 km[3], while the shadow height was above 270 kms. This fact, coupled with the vibrational and rotational temperatures of N_2 in mid-day aurora that are observed to be much higher than those found by investigators in the cases involving resonant scattering of solar radiation, suggests that resonant scattering may not be the sole source of the N_2^+ING emissions in mid-day auroras.

Another likely mechanism is that of excitation by slow ions. Earlier I mentioned that Winnigham and Heikkila[2] observed 1keV protons in the cusp region and the airborne photometer measurements in mid-day auroras detected about 10R of H_β in the mid-day auroras. Using Eather's[10] value of 1 H_β photon

for every 10 protons we get a flux of 10^8 protons/cm.^{2}/sec. With such a large flux of protons it is feasible to excite enough N_2 into the $B^2\Sigma_u^+$ state of N_2^+ to produce a detectable intensity of N_2^+1NG emissions. Moore and Doering's laboratory measurements of the ratios of the N_2^+1NG band as a function of proton energies predict an intensity ratio of 12 for the (0-0) to (1-1) bands excited by 1 keV protons. The observed intensity ratio corresponds to excitation by protons with energies of 100 to 350 eV. This does not contradict the satellite measurements which show proton energies of 1 keV since such protons may be more effective in exciting 1NG bands when they have slowed down from 1 keV to several hundred electron volts. Moore and Doering[11] also observed a rotational temperature of 3500°K in ion excited N_2^+1NG bands. However, this high temperature applies only to rotational levels with K values of greater than 22, the lower rotational levels giving much smaller rotational temperatures. On the other hand, the mid-day auroral observations show very high rotational temperatures even for low rotational levels.

At this stage of analysis it is difficult to single out the most important mechanism for the N_2^+1NG emissions in mid-day aurora. Further analysis of this data together with other measurements from a couple of other flights in the cusp region may enable us to determine the relative significance of each of the three mechanisms, discussed here, in the mid-day auroras.

REFERENCES

1. G. G. Sivjee, Analysis of Auroral Data from NASA's 1968 and 1969 Airborne Auroral Expeditions, Semi-Annual Report on NASA/AMES Grant No. NGR 02-001-099, Suppl. No. 1, Geophys. Inst., Univ. of Alaska, June, 1973.

2. W. J. Heikkila and J. D. Winningham, Penetration of magnetosheath plasma to low altitudes through the dayside magnetospheric cusps, J. Geophys. Res., 76, 883 (1971).

3. M. H. Rees, Note on the Penetration of Energetic Electrons into the Earth's Atmosphere, Planet. Space Sci., 12, 722 (1964).

4. C. G. Walker, R. S. Stolarski and A. F. Nagy, The Vibrational Temperature of Molecular Nitrogen in the Thermosphere, Ann. Geophys., 25, 831 (1969).

5. E. Jamshidi, Vibrational Temperature of N_2 in the E and F region, Master's Thesis, Wayne State Univ., 1971.

6. E. Bauer, R. Kummler and M. H. Bortner, Internal Energy Balance and Energy Transfer in the Lower Thermosphere, Appl. Optics, 10, 1861 (1971).

7. E. L. Breig, M. E. Brennan and R. J. McNeal, Effect of Atomic Oxygen on the N_2 Vibrational Temperature in the Lower Thermosphere, J. Geophys. Res., 78, 1225 (1973).

8. A. Vallance Jones and D. M. Hunten, Rotational and Vibrational Intensity Distribution of the First Negative N_2^+ Bands in Sunlit Auroral Rays, Can. J. Phys., 38, 458 (1960).

9. A. L. Broadfoot and D. M. Hunten, N_2^+ Emission in the Twilight, Planet. Space Sci., 14, 1303 (1966).

10. R. H. Eather, Auroral Proton Precipitation and Hydrogen Emissions, Rev. Geophys., 5, 207 (1966).

11. J. H. Moore, Jr., and J. P. Doering, Vibrational Excitation in Ion-Molecule Collisions: H^+, H_2^+, He^+, N^+, N_e^+, and Electrons on N_2, Phys. Rev., 177, 218 (1969).

N74-22038

OPTICAL AURORA AND ITS RELATIONSHIP TO MEASUREMENTS FROM SATELLITES, VHF RADAR AND INCOHERENT SCATTER RADARS

G. J. Romick

Geophysical Institute
University of Alaska
Fairbanks, Alaska 99701

Invited Paper given at the IAGA General Assembly in Kyoto, Japan,
September 10-21, 1973

INTRODUCTION

Papers previously presented in this session and in others yesterday have discussed many different coordinated programs and their results. Here, I will attempt to classify the types of coordinated programs that are possible and illustrate some of them with a few examples that have taken place in Alaska during the last few years.

In general there are three classes of coordinated programs. Each is illustrated in Table 1, listed in order of increasing relationship between the cooperating groups or individuals. Coincident data acquisition programs refer to the gathering of data from different instruments which by chance were operated during a particular event. The resultant analyses combine the available data to more completely describe the event. Much of the past analysis of ground and satellite data or satellite to satellite data falls in this category. Although at times frustrating and time consuming, the results of these types of coordinated analyses are quite useful.

Scheduled data acquisition from numerous instruments in operation requires collaboration among individuals prior to the occurrence of a particular event. Many of the coordinated studies today use this scheme. Satellite emphemeris data are made available to ground based experimenters and coordination of ground observations with known rocket launches, aircraft flights, and satellite overpasses are planned. Similarly, involvement of radars, and other instruments used to record magnetic activity are included in this type of program before a particular series of observations.

Planned experiments represent the direction of future programs.

Large scale programs involving the coordination of different groups to attack specific problems are being planned and observations using specific instruments for specific information are being contemplated. The A-E satellite illustrates this concept. The whole space shuttle observatory concept is being planned using this approach not only on board the satellite, but between the satellite and ground stations as well. As examples of some of these types of programs I will present some that have occurred in recent years and describe one particular study in somewhat greater detail.

Figure 1 illustrates the various major facilities in Alaska used for auroral studies in the last few years. Other ground stations north of Fort Yukon are not indicated on this map but also provide routine data such as all-sky camera photographs, 3 component magnetometer observations and riometer information primarily under the guidance of various principal investigators at the Geophysical Institute. There are also many geophysical parameters measured at the Institute that are not included in this figure but which aid in the assessment of the geophysical environment surrounding a particular event.

In many ways it is obvious that the operation of all of the facilities indicated in Figure 1 to their maximum capability would require an enormous staff. In this regard it is of interest to note in Table II the various groups which through the 1971-1973 period have been active in coordinated studies using these facilities. Not all of these groups have made simultaneous measurements and even within this small community some of the interrelationships fall under the coincidence category. However, the expertise, equipment and funding represented by this group is certainly

larger than that of any single organization and the need for coordinated efforts is plain.

Discussion of Various Programs

In many of the studies associated with the various facilities in Alaska, we use optical triangulation techniques to determine the position of the aurora in order to place the other measurements in the perspective of the overall auroral morphology (Romick & Belon, 1967). The optical data used for this purpose is either that from the meridian scanning photometer at one of the prominent auroral emissions (5577 OI or 4278 N_2^+), or the All-Sky Camera. Figure 2 shows the simple triangulation geometry in a geomagnetic meridian plane through two stations and illustrates how both height, latitude and perhaps even the vertical luminosity profile can be obtained. The use of this technique is illustrated in Figure 3, where we have plotted the location versus time of all discrete peaks of auroral 5577 OI luminosity seen along the meridian on March 9, 1972. Also indicated are the times when either rockets or satellites acquired data in the vicinity of the field stations. The local magnetic K index is also indicated. Notice that one can immediately tell in what type of activity the events occurred and what type of auroral activity immediately preceded or followed the measurements. Poleward and equatorward expansions in the evening sector are obvious in this type of plot. Another example of a different day is shown in Figure 4. The equatorward motion and rapid poleward expansion are quite easily seen. Figure 5 shows the all-sky camera pictures covering the same period as in Figure 4, and illustrates that the rapid poleward expansion was due to a westward traveling surge moving through the meridian. Figure 6 shows the relationship of the Chatanika Incoherent Scatter Radar in this event to the visual aurora. The amplitude of the electron density

is plotted along the field line intersection with the radar beam and shows how well the peaks in electron density match the auroral forms within the beam throughout the period. We are still in the process of comparing the details of the electron density to the observed optical data at various wavelengths.

Another type of study is shown in Figure 7, Romick and Sharp 1972. This illustrates a satellite pass across Alaska and the regions of precipitation measured by the satellite. The oval was deduced by the ground magnetometer data. Optical Hβ, 4278, 5577, and 6300 data from the ground were also obtained. Figure 8 shows the energy flux detected on board the satellite, and illustrates the typical evening sector morphology relating the incident protons and electrons across the oval and the position of the > 130 kev electron trapping boundary. From these satellite proton data we have calculated the Hβ intensity which should be observed. Figure 9 compares the calculated values with those actually seen after correction for scattering, extinction and path length effects. The relationship is quite good and indicates that present theory is adequate to explain the emission considering the present state of our ability to perform absolute calibrations of both particle detectors and optics independently.

Another type of coordinated experiment in which numerous instruments participated occured on March 16, 1972 Hunsucker, et al., 1972. Figure 10 contains a portion of the data that shows the comparison of the electron density measured by AFCRL on a rocket by two different techniques and that measured by the Chatanika incoherent scatter radar. As seen, the comparison is quite good over the whole altitude range. There are many other coordinated studies that are going on involving the various groups previously indicated.

The remainder of this presentation will concentrate on one preliminary study, in which I am particularly interested. It involves coordination of the analysis of data from a satellite, VHF radar and optical and magnetic observations (Romick, et al 1973). Figure 11 presents six all sky camera photographs during the passage of satellite 1971-89a which was instrumented with particle detectors by Lockheed Palo Alto Research Laboratory. Of particular interest here is the >130 kev electron detectors and the C and I boundaries which refer respectively to the cosmic ray background and the boundary where the 20^{o} and 90^{o} pitch angle detector fluxes were equal (isotropic). The radar echo is that obtained by the 50 mHz NOAA radar in Anchorage. The optical data were obtained by the Geophysical Institute at Ester Dome or Fort Yukon, Alaska. During the spring of 1972, there were nine simultaneous radar-satellite events and in all cases the radar echo was equatorward of the C trapping boundary. On three events, the range in the diffuse echo lay between the C and I boundaries. Notice the difference in position of the C boundary on the different All-Sky camera prints in Figure 11. On March 7, the boundary lies just equatorward of the bright arc and so also does the radar echo. On March 16, however, the C boundary and echo lie far equatorward of the bright arc. On other days the relationship is not as clear but the echo always appears equatorward of the C boundary. We can see this more clearly on the map type presentation shown in figure 12, for March 7, 9, 14 and 18. To study these events further, we decided to investigate the relationship of the trapping boundary position to substorm activity and DST. Figure 13 illustrates our findings with these preliminary set of data. The invariant latitudes of the C boundary plotted vs. Q midnight

or Q_{Local} indicates a possible relationship with before and after westward surge activity but the basic problem with the use of K type of indices is shown. One can have either high or low values of Q or K with high negative values of DST, and thus some confusion may occur. In contrast, the plots of C and I boundary position with DST indicate a clear substorm related effect in that for a given value of DST the position of the trapping boundary moves poleward after the expansive phase of the substorm. To us this implies that the motion of this boundary is a dynamic feature of the substorm and we feel that the use and correct interpretation of the VHF radar may allow us to follow this dynamic motion within individual events.

CONCLUDING STATEMENT

I have tried to illustrate through individual examples some of the results available in coordinated programs which involve satellites, radars, ground optical instrumentation, and other types of observing facilities. I hope it is clear to everyone that it will take more of these types of programs to solve the basic problems in the study of atmospheric and magnetospheric geophysics.

Table I

1) COINCIDENCE DATA ACQUISITION	COMBINED ANALYSIS
2) SCHEDULED DATA ACQUISITION	COORDINATED PROGRAMS
3) PLANNED EXPERIMENT	COORDINATED COOPERATIVE PROGRAM OF DATA ACQUISITION AND ANALYSIS

Table II

1971-1973 ALASKAN OPERATIONS

RADAR OPERATION	GROUND OPTICS	SATELLITES	ROCKETS
NOAA-BOULDER	UTAH STATE UNIVERSITY	YORK UNIVERSITY	RICE UNIVERSITY
STANFORD RESEARCH INSTITUTE	UNIVERSITY OF COLORADO	UNIVERSITY OF CALGARY	UTAH STATE UNIVERSITY
GEOPHYSICAL INSTITUTE	UNIVERSITY OF MICHIGAN	UNIVERSITY OF MICHIGAN	AIR FORCE CAMBRIDGE RESEARCH LA
	UNIVERSITY OF TEXAS, DALLAS	NASA-GODDARD	LOS ALAMOS SCIENTIFIC LAB
	YORK UNIVERSITY	LOCKHEED PALO ALTO RESEARCH LAB	UNIVERSITY OF NEW HAMPSHIRE
	LOS ALAMOS SCIENTIFIC LAB		UNIVERSITY OF MINNESOTA
	NASA-GODDARD		UNIVERSITY OF CALIFORNIA
	LOCKHEED PALO ALTO RESEARCH LAB		NASA-GODDARD
	GEOPHYSICAL INSTITUTE		GEOPHYSICAL INSTITUTE

Romick, G. J. and A. E. Belon, Spatial variation of auroral luminosity, Plan. Space Sci., 15, 475-493, 1967.

Romick, G. J. and R. D. Sharp, Correlations of satellite and ground observations of aurora on February 19, 1972 SA-53, Transact AGU, 53, November 1972.

Romick, G. J., W. E. Ecklund, B. Balsley, R. Greenwald and W. Imhof, The interrelationship between the > 130 kev electron trapping boundary, diffuse VHF radar echoes and the visual aurora, J. Geophys. Res., in press, 1974.

Hunsucker, R. D., A. H. Steinfeld, G. J. Romick, A. E. Belon, H. F. Bates, W. L. Ecklund, B. B. Balsley, R. A. Greenwald and R. Tsunoda, Structure and dynamics of ionization and auroral luminosity during the auroral display of March 16, 1972 near Chatanika, Alaska, SA-48, Transact 64, 53, November 1972.

Figure 1. Schematic representation of the distribution of various scientific facilities in Alaska

Figure 2. Triangulation geometry illustrating how the height, latitude and volume emission rate within an aurora can be deduced from two stations along a geomagnetic meridian.

Figure 3. Latitudinal positions of discrete aurora plotted versus time on March 9, 1972. Also indicated are the times of closest approach of two satellites and the times at which rockets were launched from Poker Flat Range.

Figure 4. Latitudinal position of discrete aurora plotted versus time on February 17, 1972.

Figure 5. All-sky camera photographs showing the development of a substorm as seen in the evening sector at Ft. Yukon, Alaska, corresponding to the time interval illustrated in Figure 4.

Figure 6. The Chatanika Incoherent Scatter Radar observations of electron density along the radar beam in the aurora observed in Figure 5. The amplitude of the electron density is plotted along the field line intersection the radar beam. The aurora is between the vertical lines.

Figure 7. Relationship between the observed electron and proton particle precipitation and the position of the statistical oval for the STP-71a Satellite pass on 19 February 1972 (Romick and Sharp, 1972).

Figure 8. Total proton and electron energy fluxes observed as a function of geomagnetic latitude for the satellite pass in Figure 6

Figure 9. Calculated (thin line) and observed (solid line) Hβ intersecting with corrections for path length, atmospheric extinction and scattering (dots) calculated data used the proton fluxes in Figure 8.

Figure 10. Electron density measured as a function of altitude by rocket techniques and simultaneous Incoherent Scatter Radar (Hunsucker et al., 1972).

Figure 11. All sky camera data showing the relationship between the > 130 kev electron boundaries C and J, the 50 mHz radar echoes and the visual aurora. On March 7, the lower border of the aurora north of the zenith is outlined. On March 14, the C boundary is north of the field of view of the camera. The white dots in the S, SW and SE at Ft. Yukon and Ester Dome are reflections off the plastic dome (Romick et al., 1973).

Figure 12. Maps of the relationship between the observed positions of the trapping boundaries for > 130 kev electrons, 50 mHz radar echoes, and the actual position of visible aurora at 110 km (Romick et al., 1973).

Figure 13. Plot of the invariant latitude of the 130 keV trapping boundaries [cut off (C) and isotropic (I)] versus magnetic indices using data from magnetic midnight (Q_m) or local region (Q_L) and DST and divided into before (circles) and after (dots) westward traveling surge activity (Romick et al., 1973).

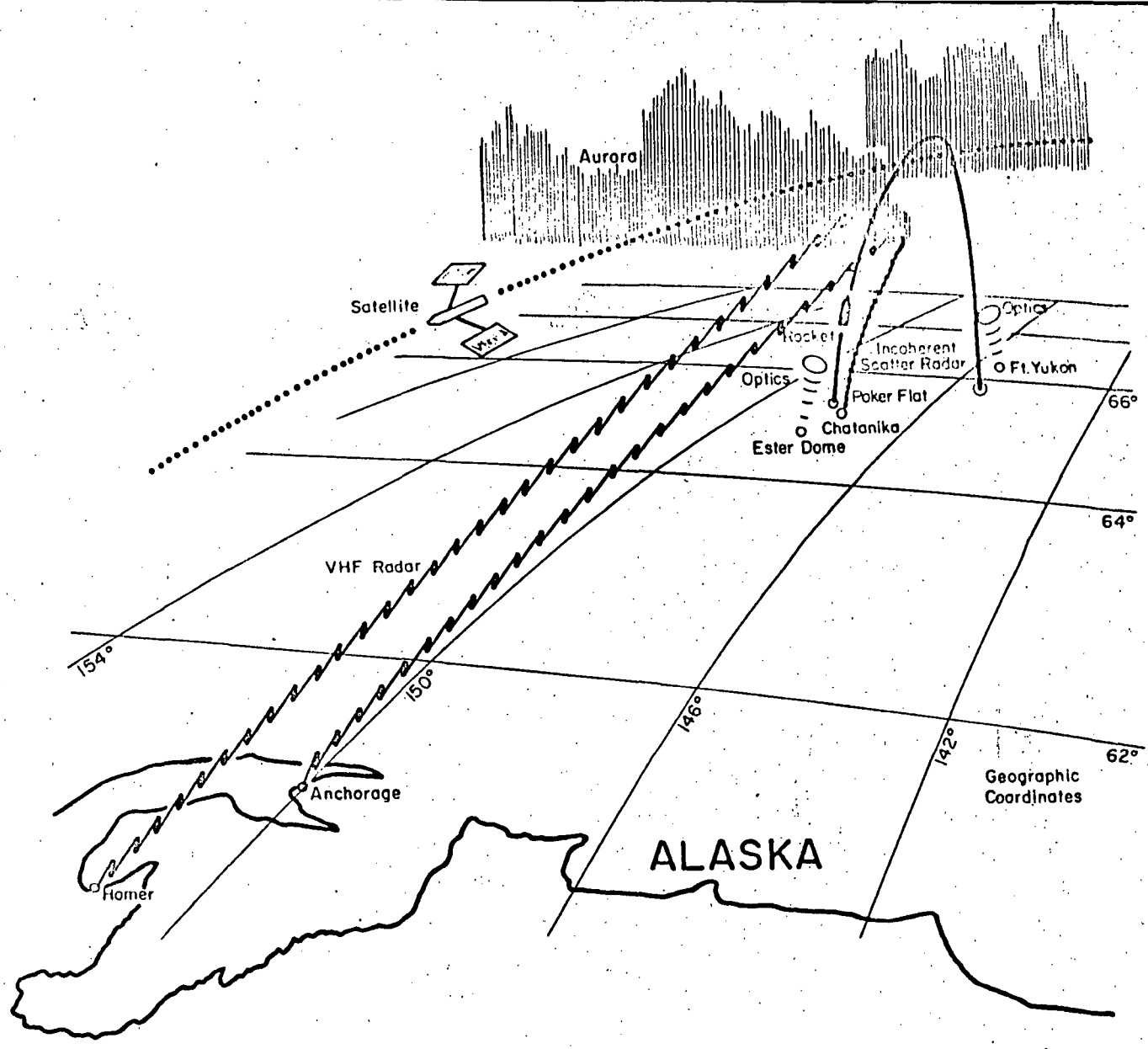

Figure 1. Schematic representation of the distribution of various scientific facilities in Alaska

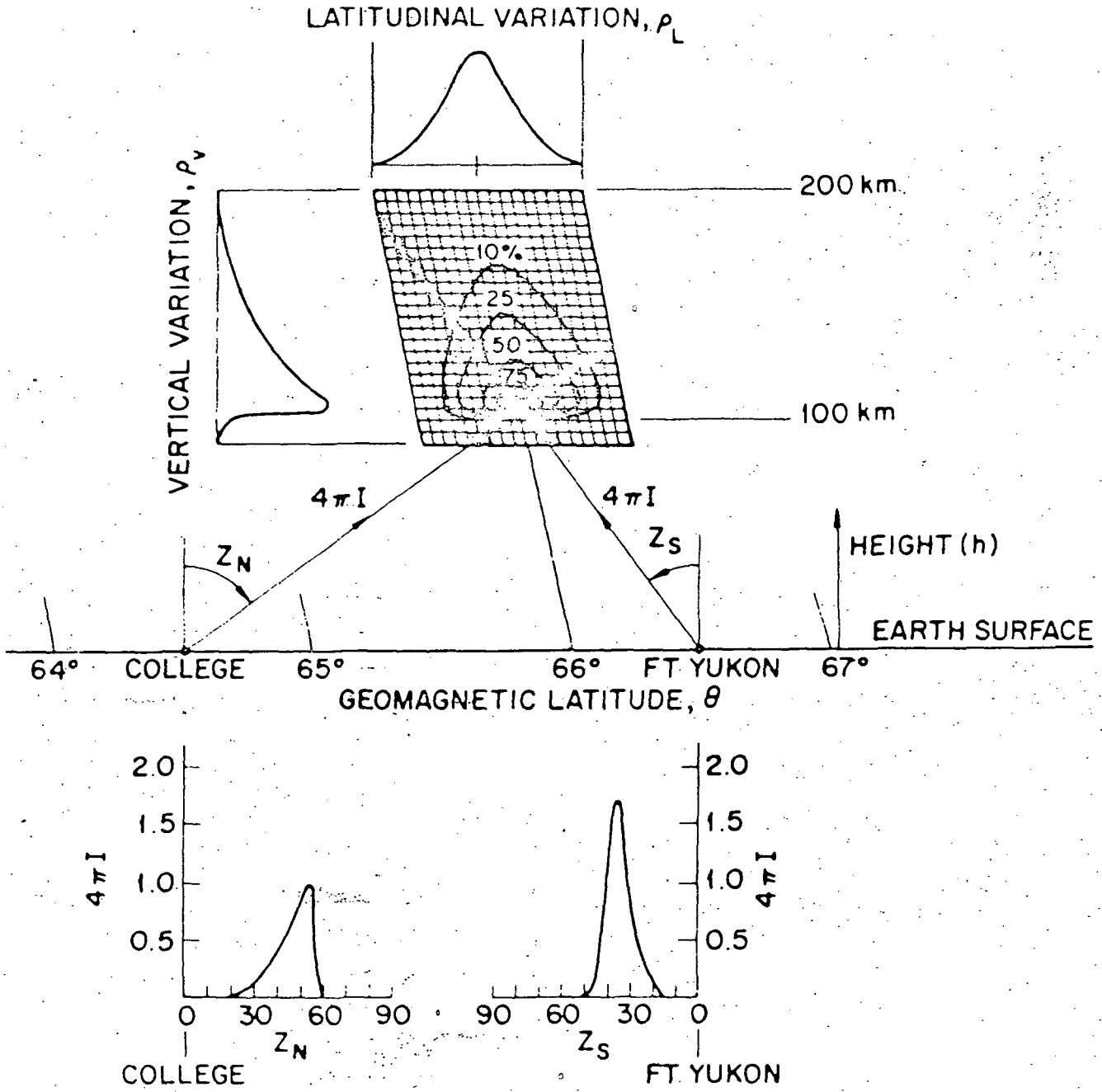

Figure 2. Triangulation geometry illustrating how the height, latitude and volume emission rate within an aurora can be deduced from two stations along a geomagnetic meridian.

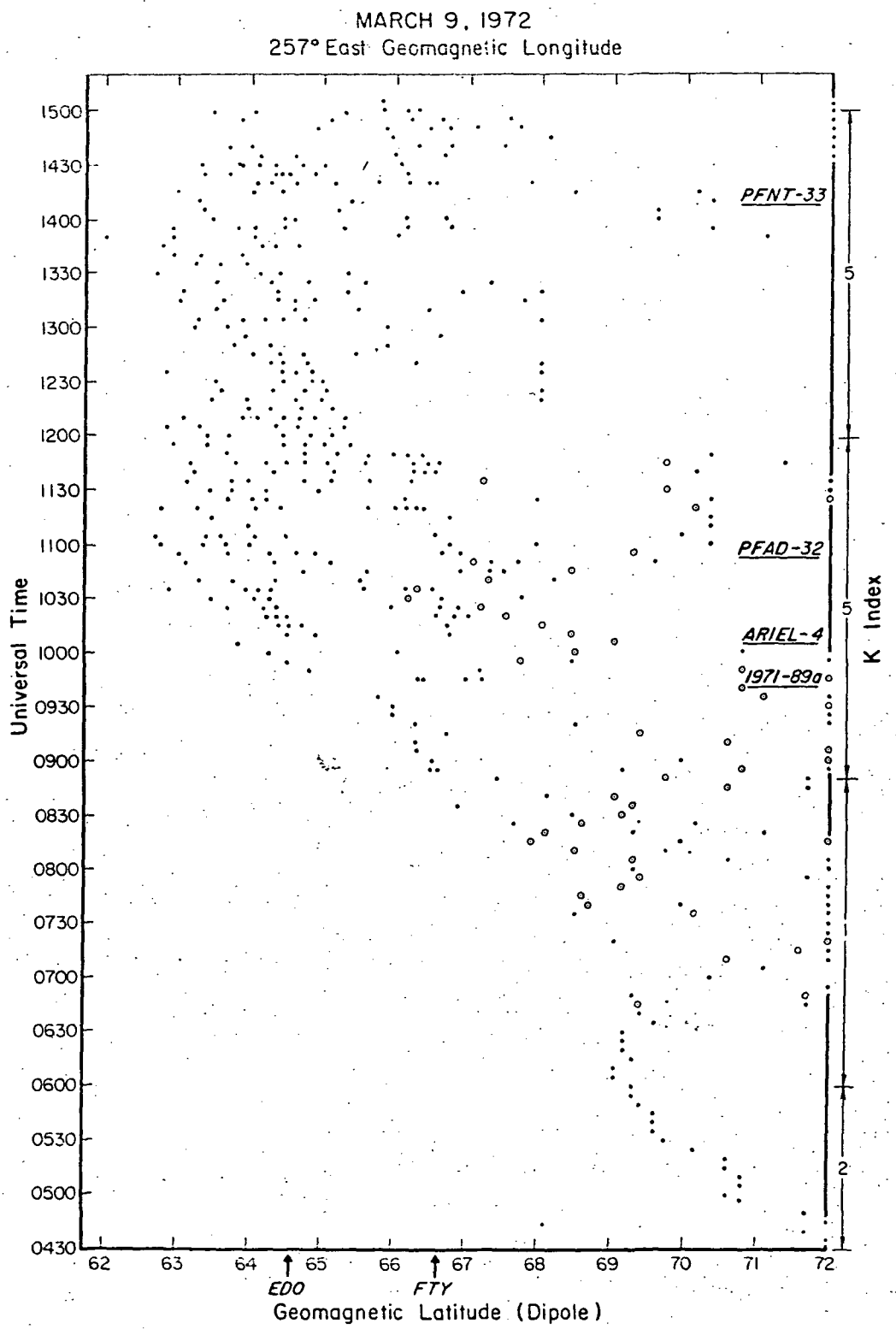

Figure 3. Latitudinal positions of discrete aurora plotted versus time on March 9, 1972. Also indicated are the times of closest approach of two satellites and the times at which rockets were launced from Poker Flat Range.

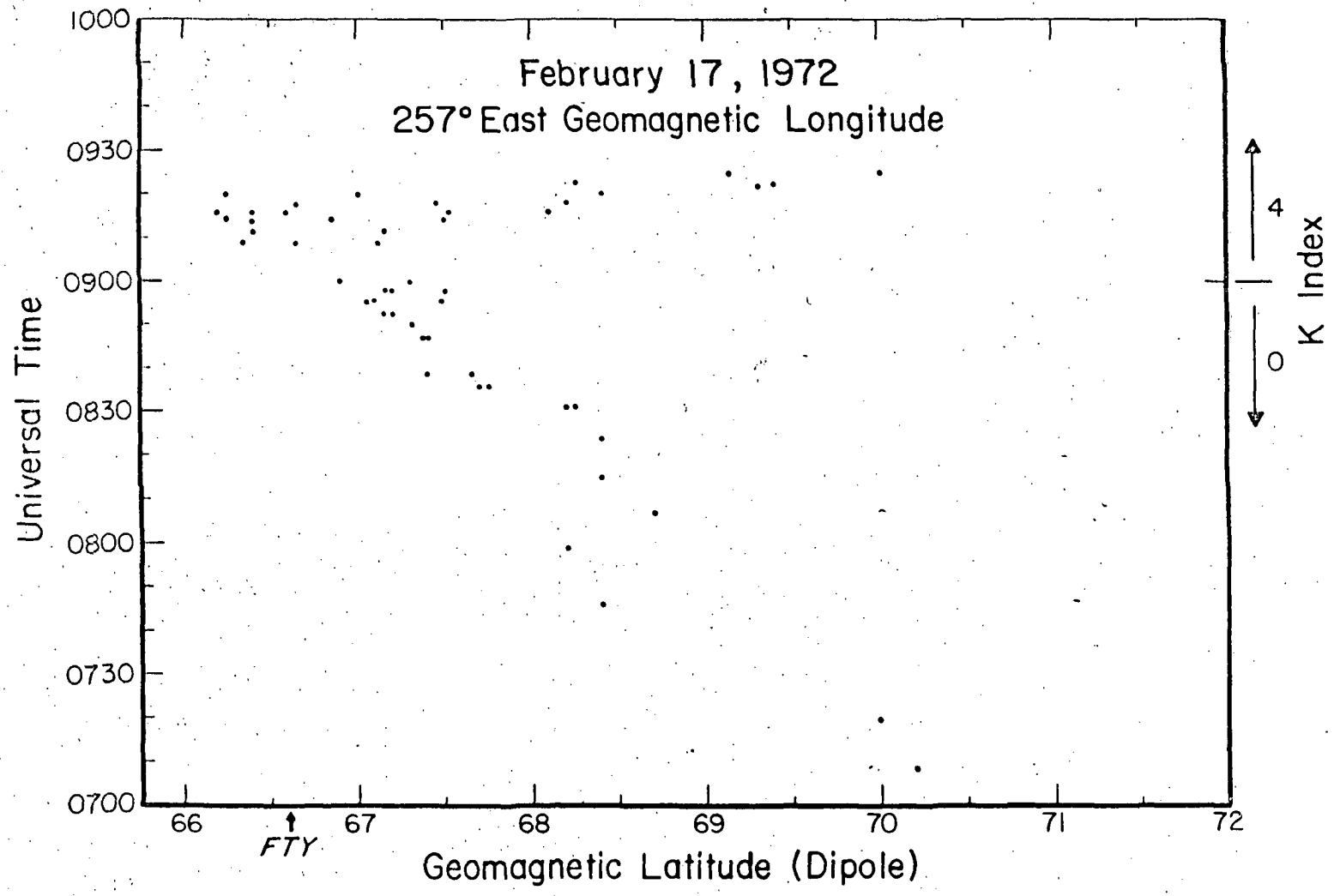

Figure 4. Latitudinal position of discrete aurora plotted versus time on February 17, 1972.

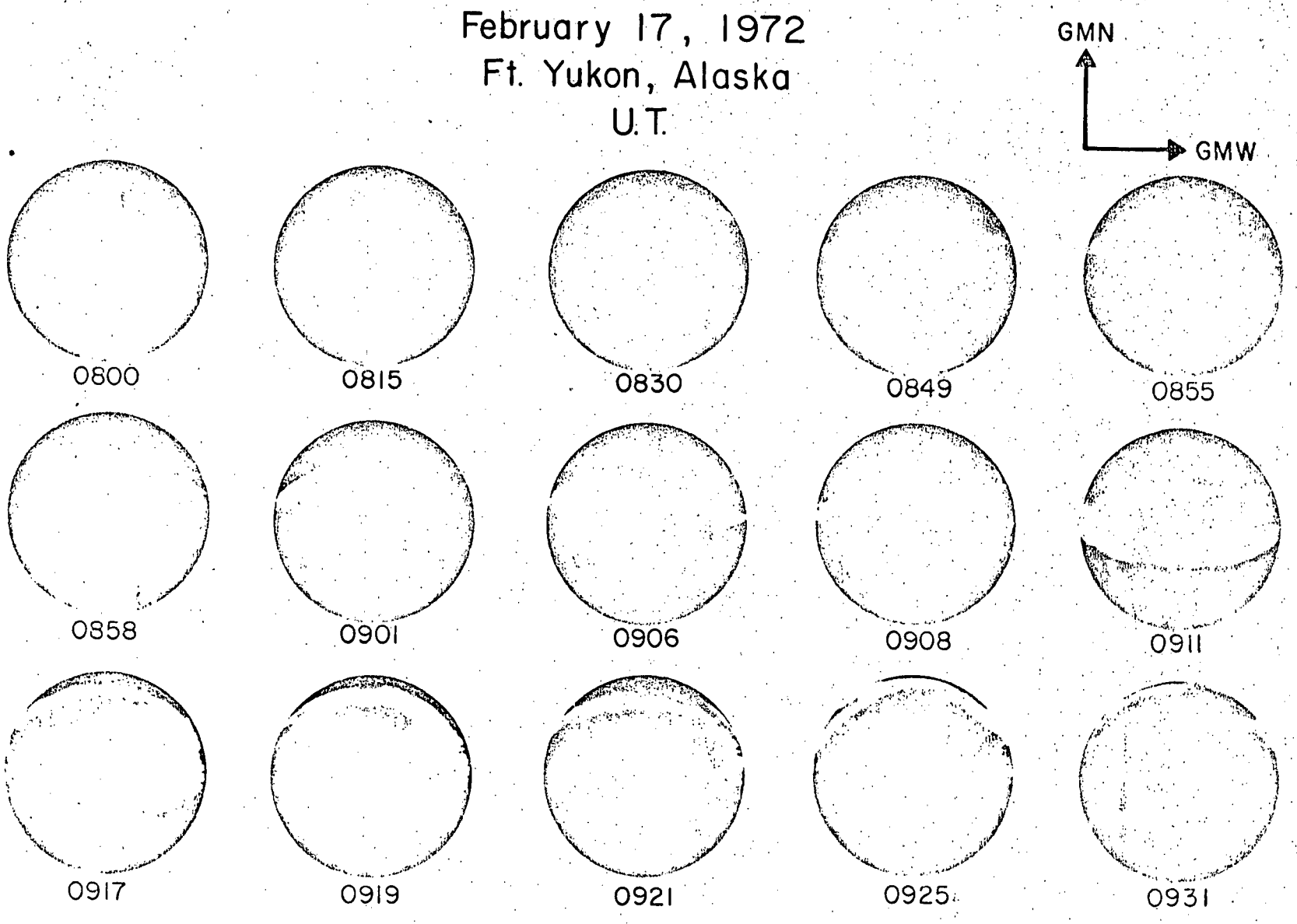

Figure 5. All-sky camera photographs showing the development of a substorm as seen in the evening sector at Ft. Yukon, Alaska, corresponding to the time interval illustrated in Figure 4.

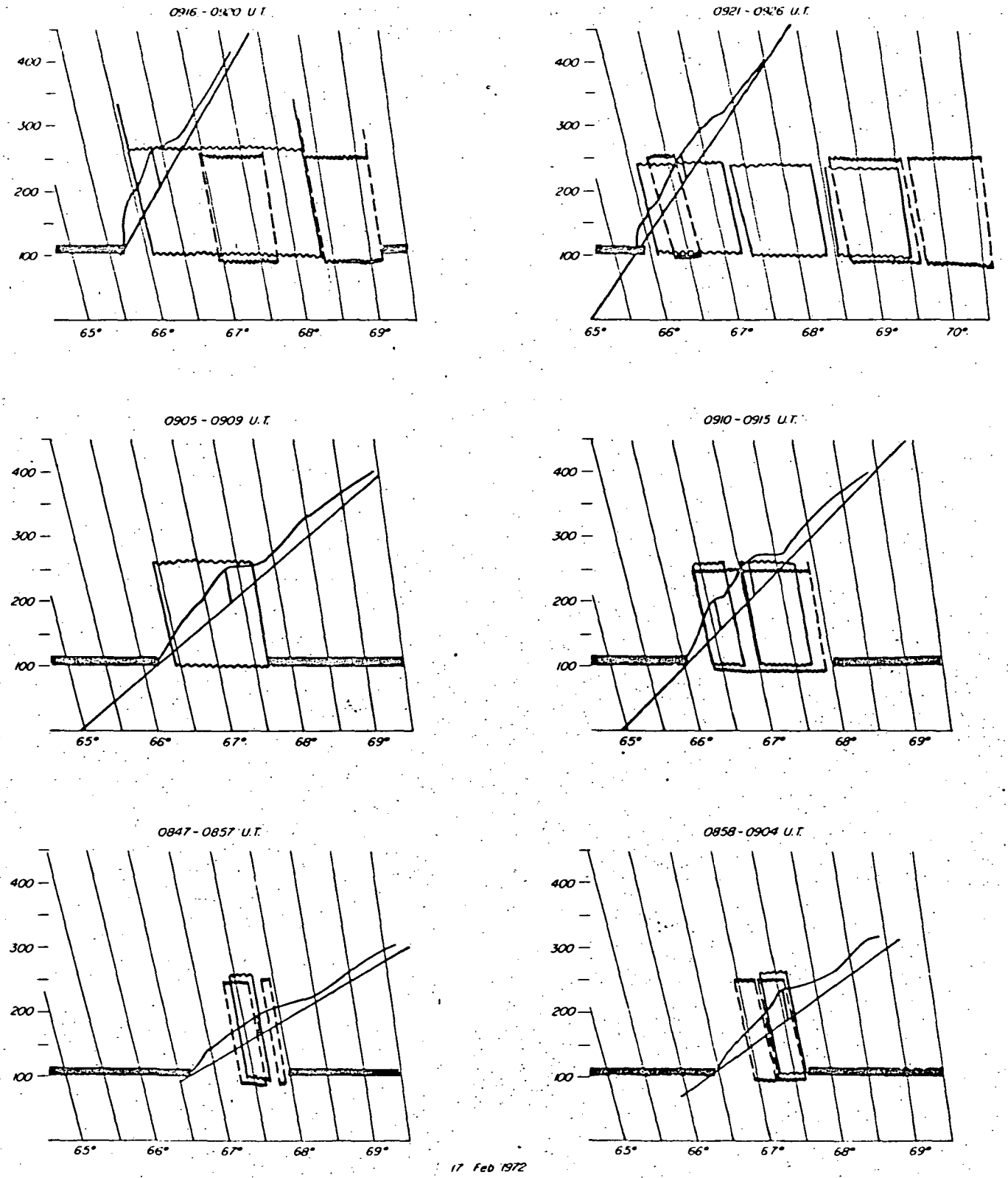

Figure 6. The Chatanika Incoherent Scatter Radar observations of electron density along the radar beam in the aurora observed in Figure 5. The amplitude of the electron density is plotted along the field line intersection the radar beam. The aurora is between the vertical lines.

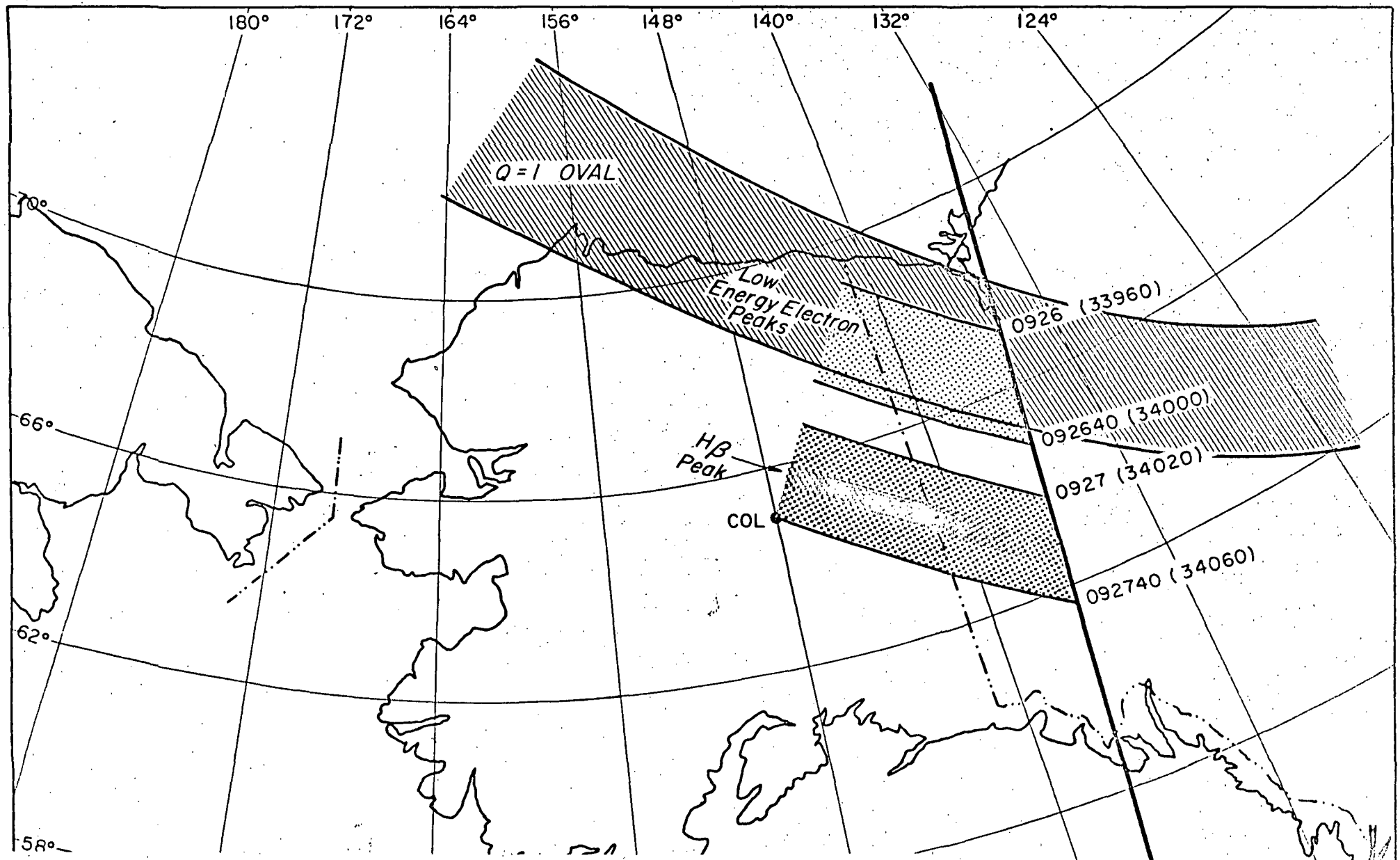

Figure 7. Relationship between the observed electron and proton particle precipitation and the position of the statistical oval for the STP-71a Satellite pass on 19 February 1972 (Romick and Sharp, 1972).

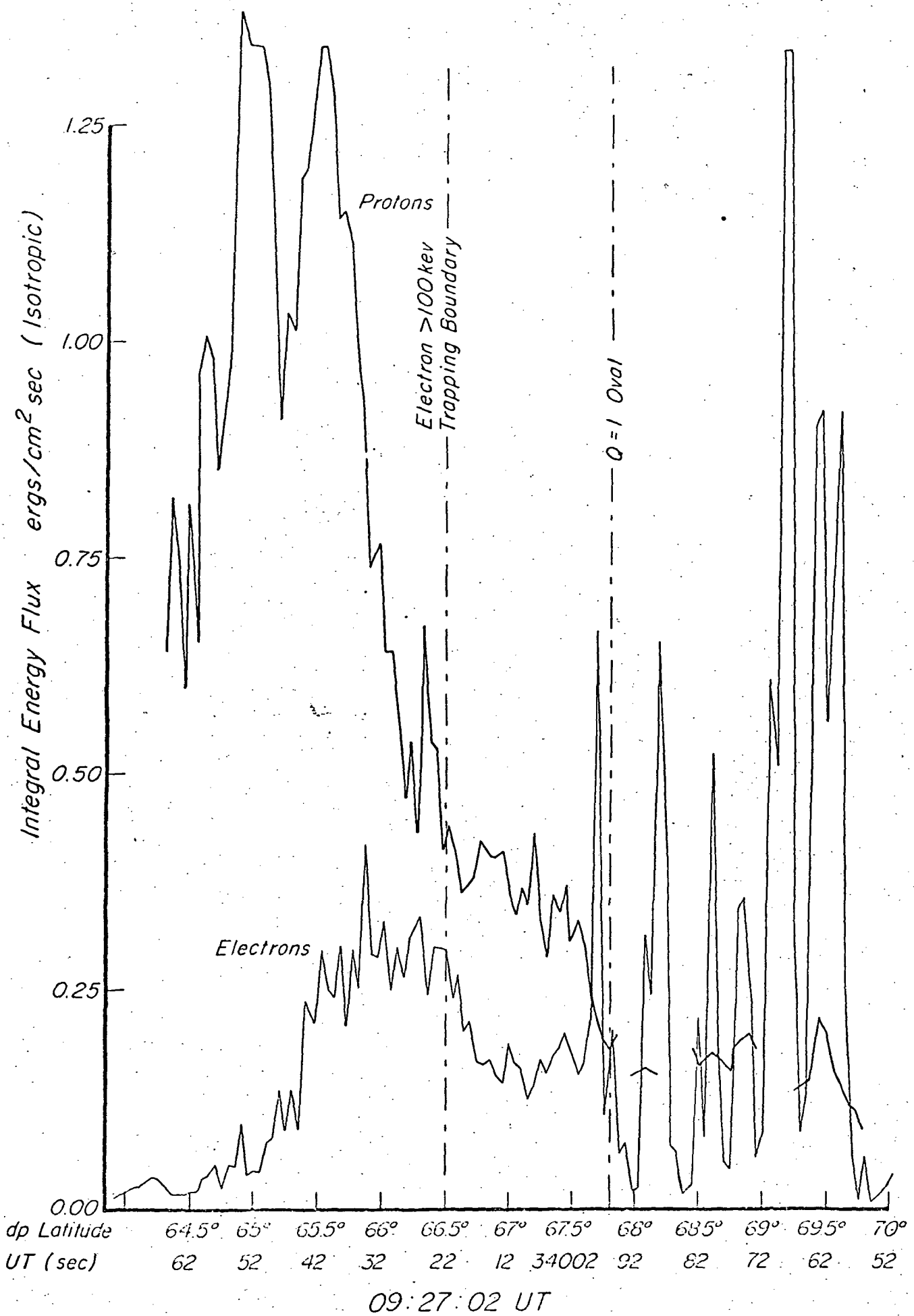

Figure 8. Total proton and electron energy fluxes observed as a function of geomagnetic latitude for the satellite pass in Figure 6

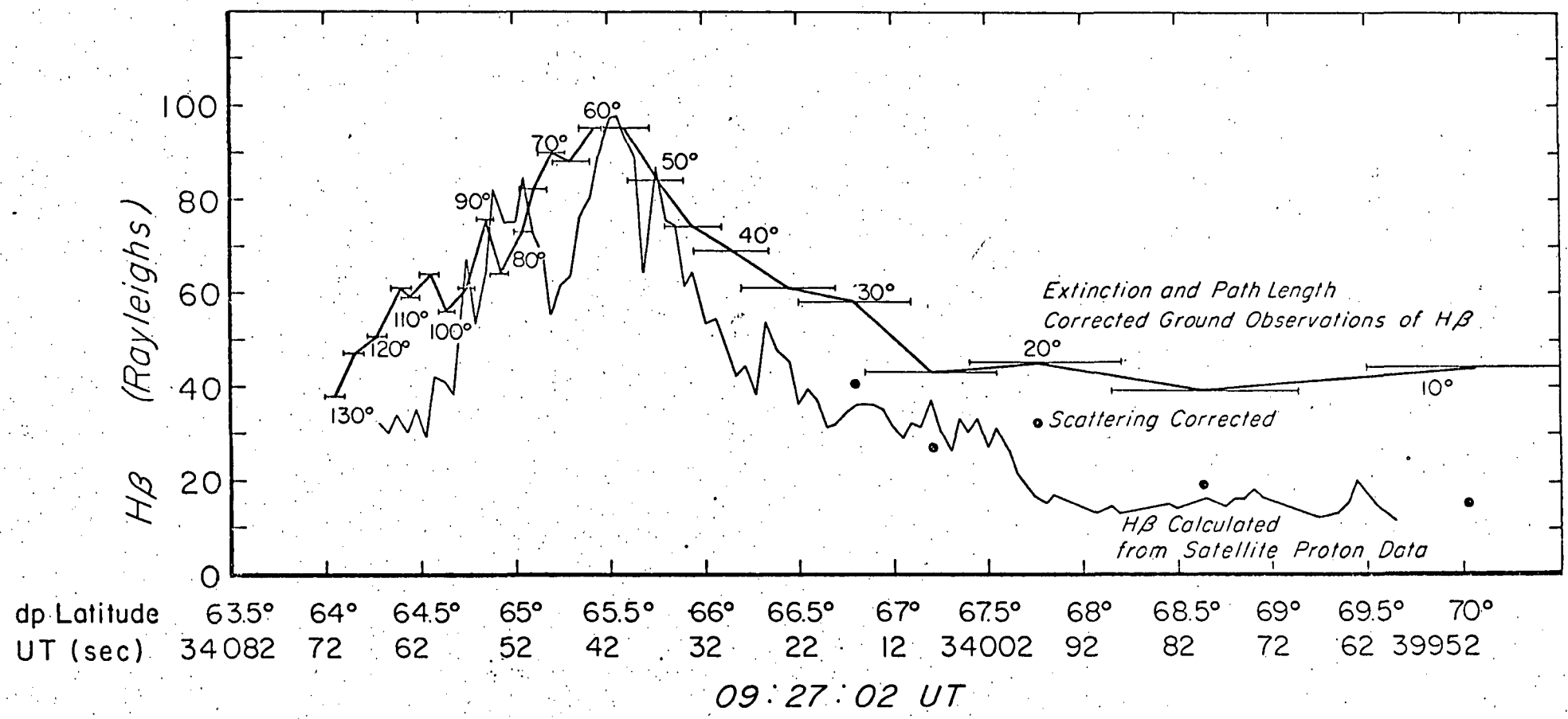

Figure 9. Calculated (thin line) and observed (solid line) Hβ intersecting with corrections for path length, atmospheric extinction and scattering (dots) calculated data used the proton fluxes in Figure 8.

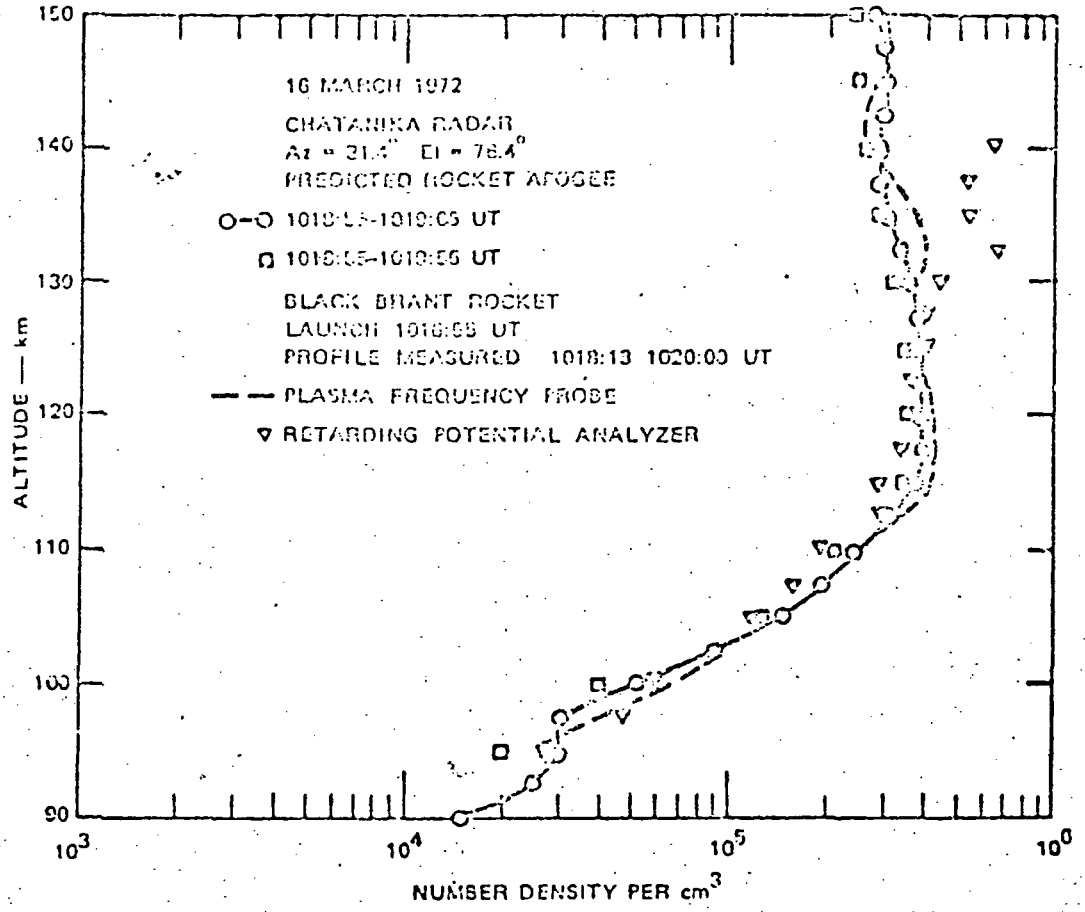

Figure 10. Electron density measured as a function of altitude by rocket techniques and simultaneous Incoherent Scatter Radar (Hunsucker et al., 1972).

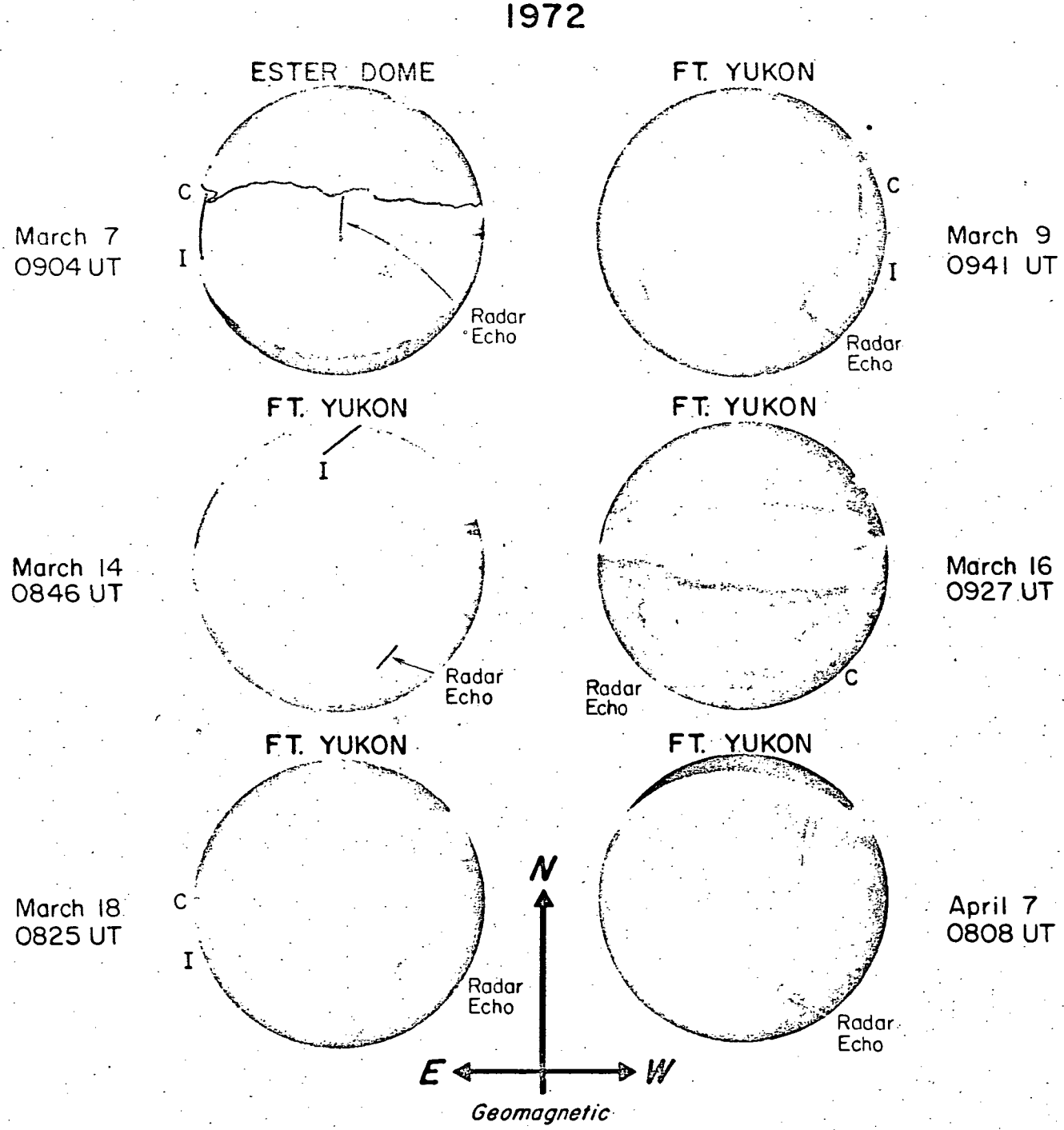

Figure 11. All sky camera data showing the relationship between the > 130 kev electron boundaries C and J, the 50 mHz radar echoes and the visual aurora. On March 7, the lower border of the aurora north of the zenith is outlined. On March 14, the C boundary is north of the field of view of the camera. The white dots in the S, SW and SE at Ft. Yukon and Ester Dome are reflections off the plastic dome (Romick et al., 1973).

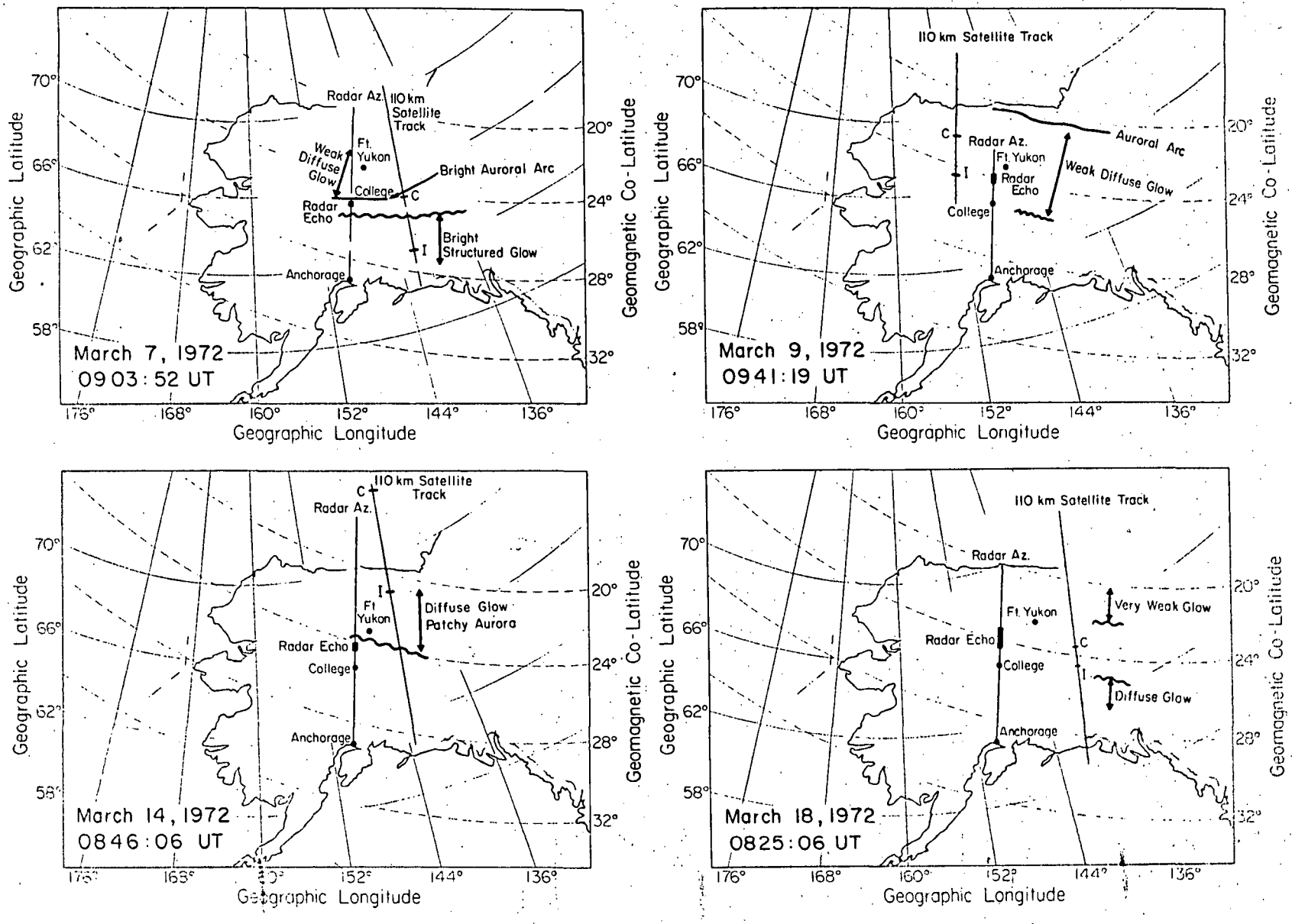

Figure 12. Maps of the relationship between the observed positions of the trapping boundaries for > 130 kev electrons, 50 mHz radar echoes, and the actual position of visible aurora at 110 km (Romick et al., 1973).

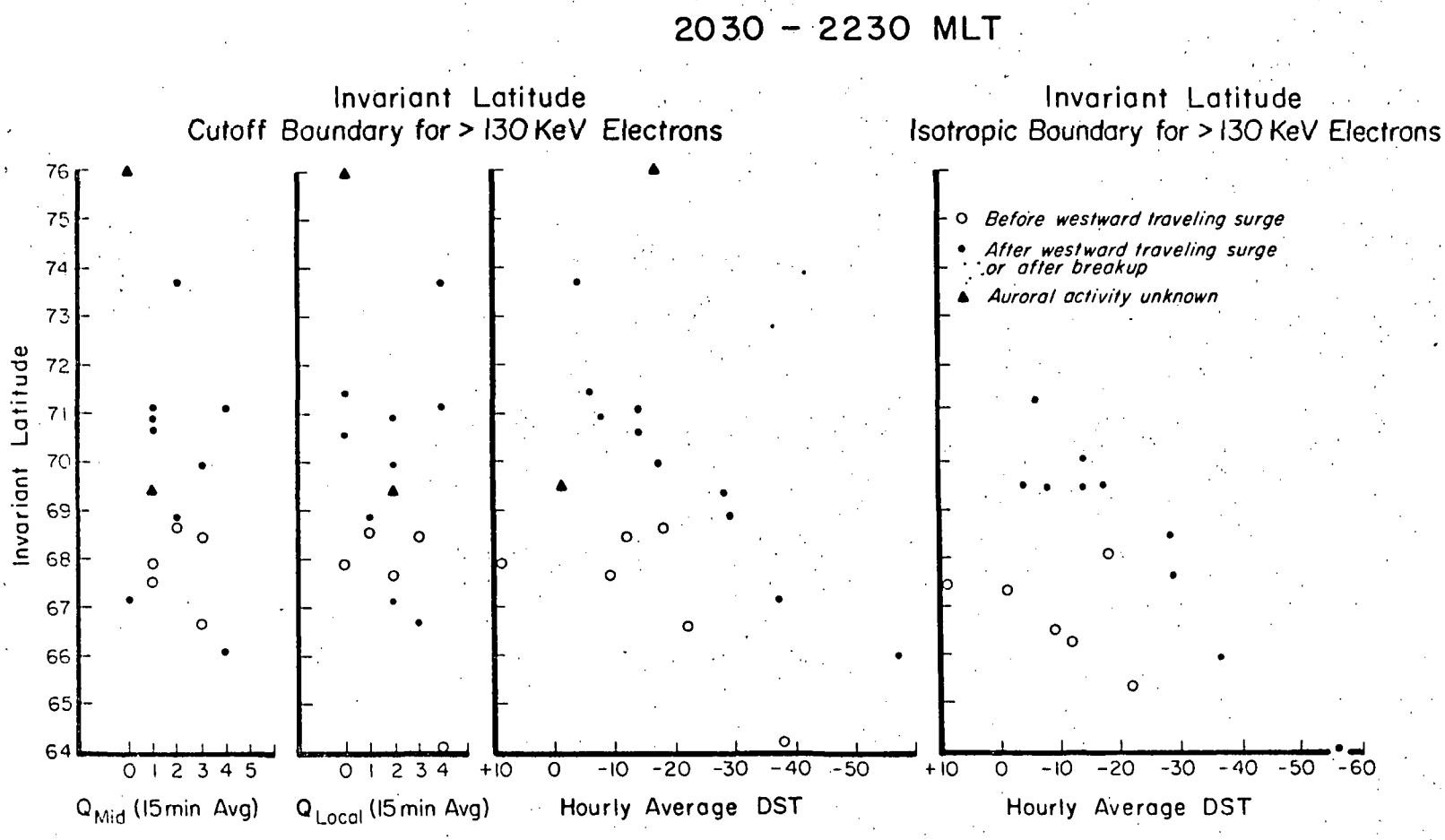

Figure 13. Plot of the invariant latitude of the 130 keV trapping boundaries [cut off (C) and isotropic (I)] versus magnetic indices using data from magnetic midnight (Q_m) or local region (Q_L) and DST and divided into before (circles) and after (dots) westward traveling surge activity (Romick et al., 1973).